Available online at www.sciencedirect.com
ScienceDirect
Journal of Magnetism and Magnetic Materials 310 (2007) 116–125
Journal of magnetism and magnetic materials
www.elsevier.com/locate/jmmm

Equilibrium magnetisation structures in ferromagnetic nanorings

Volodymyr P. Kravchuk[a], Denis D. Sheka[a,*], Yuri B. Gaididei[b]

[a]National Taras Shevchenko, University of Kiev, 03127 Kiev, Ukraine
[b]Institute for Theoretical Physics, 03143 Kiev, Ukraine

Received 8 April 2006; received in revised form 10 July 2006
Available online 1 September 2006

Abstract

The ground state of the ring-shape magnetic nanoparticle is studied. Depending on the geometrical and magnetic parameters of the nanoring, there exist different magnetisation configurations (magnetic phases): two phases with homogeneous magnetisation (easy-axis and easy-plane phases) and two inhomogeneous (planar vortex phase and out-of-plane one). The existence of a new intermediate out-of-plane vortex phase, where the inner magnetisation is not strongly parallel to the easy axis, is predicted. Possible transitions between different phases are analysed using the combination of analytical calculations and micromagnetic simulations.

PACS: 75.75.+a; 75.40.Mg; 75.30.Kz

Keywords: Magnetic nanoparticle; Vortex state; Uniform state; Nanodots and nanoring; Micromagnetic simulations

1. Introduction

Magnetic nanoparticles and their structures have become a subject of interest in the past few years [1]. For nanoparticles of axial geometry, such as disks (*nanodots*) and rings (*nanorings*), the vortex configuration becomes the lowest energy state when the particle diameter exceeds the single-domain size owing to the competition between exchange and magnetostatic interactions [2]. Because of nontrivial topological properties, the vortex state nanoparticles are promising candidates for the high-density magnetic storage devices, some designs of magnetic memories and high-resolution magnetic field sensors [3].

There are known two types of vortices in nanomagnetism. For a disk-shaped particle there exists an out-of-plane vortex (OPV), which is characterised by the core magnetisation perpendicular to the disk plane. Different static and dynamical properties of magnetic nanodisks have been studied recently. In particular, theoretical and experimental studies of the transition between single domain and vortex configurations (phases) [3–7] give a possibility to conclude, that the vortex state in a nanodisk can exist for the dot diameter in the submicron range, which is much more than the minimum nanoparticle size, currently used in experiments. That makes serious limitations for considering such structure as competitive one for the magnetisation storage.

The ring shape potentiates more magnetisation configurations, see for review Ref. [8]. It is well-known [8] that the pure in-plane vortex (IPV) configuration can be realised in a nanoring, where the perpendicular magnetisation component is absent. Such a vortex has lower energy than the OPV in a disk, it does not produce surface magnetostatic charges, thus it can provide more stable magnetic bit for the magnetisation storage.

Since there exist pure OPV for the disk and pure IPV for the ring, there appears a reasonable question, whether the intermediate state exists or not. We will show in the paper that *intermediate vortices* (IMVs) exist in the nanoring when the inner hole is small enough. For such vortices the magnetisation inside the vortex core has an out-of-plane component, but even in the vortex centre it is not perpendicular to the ring plane. The presence of the hole in the disk decreases the "singularity" in the vortex centre and so it gives an opportunity to realise the vortex state in a

*Corresponding author. Tel.: +380 44 526 0583; fax: +380 44 289 8391.
E-mail address: denis_sheka@univ.kiev.ua (D.D. Sheka).

0304-8853/$ - see front matter © 2006 Elsevier B.V. All rights reserved.
doi:10.1016/j.jmmm.2006.07.035

smaller nanoparticle. We will demonstrate that the vortex state can be realised in a nanoring with diameter of few tens of nanometers.

In this paper we provide the systematic study of the magnetic nanoring's ground state. Namely, by combining analytical methods and micromagnetic simulations we describe the equilibrium magnetic phases: two homogeneous states with magnetisation directions along the ring plane and perpendicular to it, and inhomogeneous vortex states, including OPV, IPV, and IMV states. The key moment is to propose the simple analytical approach, which allows us to describe different states and transitions between them.

The paper is organised as follows. In Section 2 we formulate the model and treat it analytically for the homogeneously magnetised nanoring. The vortex-state nanorings are analysed in Section 3 both analytically, using simple two-parameter ansatz, and numerically, using micromagnetic simulations. The phase diagram of possible ground states compares analytical predictions and numerical simulations (Section 4).

2. The model. Homogeneous states

We start with the continuum description of the spin distributions inside the nanoring in terms of the magnetisation, normalised by its saturation value, $\boldsymbol{m} = \boldsymbol{M}/M_s$, and content ourselves with two main contributions to the energy functional, the exchange energy E_{ex} and the magnetostatic energy E_{MS}. We neglect the anisotropy energy contributions, what is a reasonable for the soft materials like permalloy ($Ni_{80}Fe_{20}$, Py).

For the homogeneous magnetisation distribution the total energy contains only the contribution of surface magnetostatic charges:

$$E_{MS} = \frac{1}{2}\int_S \int_{S'} \frac{(\boldsymbol{M}\cdot \mathrm{d}\boldsymbol{S})(\boldsymbol{M}'\cdot \mathrm{d}\boldsymbol{S}')}{|\boldsymbol{r}-\boldsymbol{r}'|}. \tag{1}$$

Let us consider the nanoring, R is the outer radius, a is its inner radius, and h is the thickness. First of all we study the case of the ring homogeneously magnetised along its plane. It is convenient to consider the energy density, normalised by the value $\pi R^2 h M_s^2$:

$$W_{MS} = \frac{\varepsilon}{\pi}\int_S \int_{S'} \frac{\rho\,\mathrm{d}\chi\,\mathrm{d}\zeta\rho'\,\mathrm{d}\chi'\,\mathrm{d}\zeta'\cos\chi\cos\chi'}{\sqrt{\rho^2+\rho'^2-2\rho\rho'\cos(\chi-\chi')+4\varepsilon^2(\zeta-\zeta')^2}},$$

where S indicates the outer and inner edge surfaces, (ρ,χ,ζ) are the cylindrical coordinates, ρ is the radius normalised by the magnitude of the outer ring radius R, the variable ζ is the thickness normalised by h. We have introduced also the particle *aspect ratio* $\varepsilon = h/2R$, and *radii ratio* $\alpha = a/R$. Integration over edge surface can be rewritten in explicit form:

$$W_{MS}^x = \mathscr{E}(1,1) - 2\alpha\mathscr{E}(1,\alpha) + \alpha^2\mathscr{E}(\alpha,\alpha),$$

$$\mathscr{E}(\rho,\rho') = \frac{\varepsilon}{\pi}\int_0^{2\pi}\mathrm{d}\chi'\int_0^1\mathrm{d}\zeta\int_0^1\mathrm{d}\zeta'\int_0^{2\pi}\mathrm{d}\chi \times \frac{\cos\chi\cos\chi'}{\sqrt{\rho^2+\rho'^2-2\rho\rho'\cos(\chi-\chi')+4\varepsilon^2(\zeta-\zeta')^2}}. \tag{2a}$$

Straightforward but long and tedious calculations result

$$\mathscr{E}(\rho,\rho) = \frac{4\rho}{3\varepsilon}\left\{-1+\frac{1}{m}\left[\frac{\varepsilon^2}{\rho^2}\mathrm{K}(m)+\left(1-\frac{\varepsilon^2}{\rho^2}\right)\mathrm{E}(m)\right]\right\}, \tag{2b}$$

$$\mathscr{E}(1,\alpha) = \frac{\sqrt{1+\alpha^2}}{2\varepsilon}I(m_1) - \frac{\sqrt{1+\alpha^2+4\varepsilon^2}}{2\varepsilon}I(m_2) + \frac{4\varepsilon}{m_2\sqrt{\alpha}}[\mathrm{K}(m_2)-\mathrm{E}(m_2)] + \frac{4\varepsilon m_2(1-m_1^2)}{m_1^2\sqrt{\alpha}}[\mathrm{K}(m_2)-\Pi(m_1^2,m_2)], \tag{2c}$$

$$I(x) = \frac{8\sqrt{1-x^2/2}}{3x^2}\left[\frac{1-x^2}{1-x^2/2}\mathrm{K}(x)-\mathrm{E}(x)\right], \tag{2d}$$

$$m = \frac{1}{\sqrt{1+\varepsilon^2/\rho^2}},\quad m_1 = \frac{2\sqrt{\alpha}}{1+\alpha},\quad m_2 = \frac{2\sqrt{\alpha}}{\sqrt{(1+\alpha)^2+4\varepsilon^2}}. \tag{2e}$$

Here $\mathrm{K}(x), \mathrm{E}(x)$ and $\Pi(x,y)$ are the complete elliptic integrals of the first, second and third kind, respectively [9].

In the limit case of the disk, the bulk expression (2) transfers into the well-known [10] formula

$$W_{MS}^{x(\mathrm{disk})} = \frac{4}{3\varepsilon}\left\{-1+\frac{1}{m}[\varepsilon^2\mathrm{K}(m)+(1-\varepsilon^2)\mathrm{E}(m)]\right\},\quad m = \frac{1}{\sqrt{1+\varepsilon^2}}. \tag{3}$$

To calculate the energy of the ring, homogeneously magnetised along z-axis, one can use relations between the magnetometric demagnetisation factors [11]. These may be written in the form

$$2W_{MS}^x + W_{MS}^z = 2\pi(1-\alpha^2), \tag{4}$$

where the factor $(1-\alpha^2)$ appears in consequence of our normalisation of the energy density.

It is well known that the homogeneously in-plane magnetised (easy-plane, EP) state is preferable energetically for thin enough disk particles; when the disk aspect ratio is greater then the critical value $\varepsilon_0 \approx 0.906$ [10], the homogeneously out-of-plane magnetised (easy-axis, EA) state is realised.

Here, we make a similar critical analysis for the nanoring. At critical values of the parameters $W_{MS}^x = W_{MS}^z$, and the critical curve $\varepsilon_c(\alpha)$ can be found by solving the equation $W_{MS}^x(\varepsilon_c,\alpha) = 2\pi/3(1-\alpha^2)$. The numerical solution of this equation is plotted in Fig. 1. For the approximate

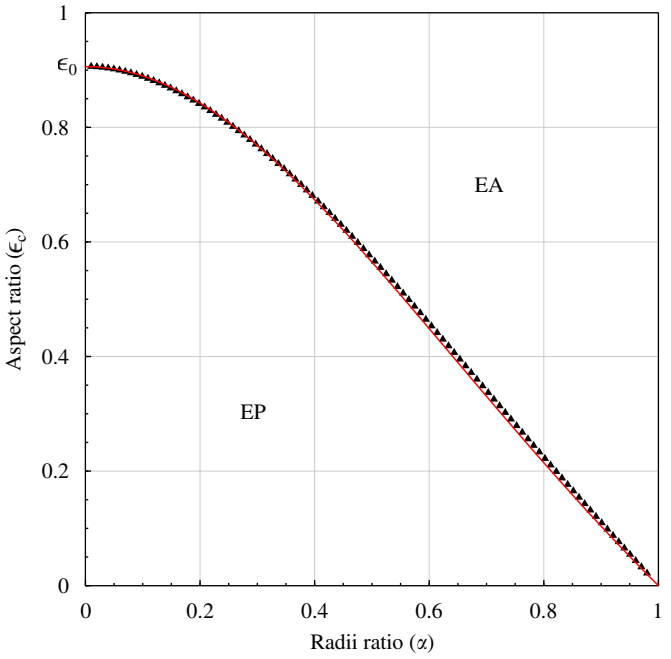

Fig. 1. The critical curve for the homogeneously magnetised states. Symbols correspond to the numerical solution (see the text), and the curve is the approximate solution (5).

description one can use the asymptotically correct solution

$$\varepsilon_c^{\text{approx}}(\alpha) = \varepsilon_0 \frac{1-\alpha^2}{1-\alpha^2+2\alpha^2\varepsilon_0}, \tag{5}$$

which reproduces the numerical results with the accuracy within 6×10^{-3}, see Fig. 1.

3. Vortex state

The phase diagram, see Fig. 1, describes the single-domain formation only. When the particle size exceeds the exchange length, $l_{\text{ex}} = \sqrt{A/4\pi M_s^2}$ (A is the exchange constant of the material), a magnetisation curling takes place [2], and the vortex-state can be energetically preferable. We start with the exchange energy in the form $E_{\text{ex}} = 1/2Ah\int \mathrm{d}^2x(\nabla \boldsymbol{m})^2$. Using the angular parametrisation for the normalised magnetisation $\boldsymbol{m} = \{\sin\theta\cos\phi; \sin\theta\sin\phi; \cos\theta\}$, one can describe the vortex solution as follows:

$$\theta = \theta(r), \quad \phi = \pm\frac{\pi}{2} + \chi. \tag{6}$$

Here, (r,χ) are the polar coordinates in the ring plane. For the vortex-like solution (6) the exchange energy density takes a form:

$$W_{\text{ex}}^{\text{vortex}} = \frac{4\pi l_{\text{ex}}^2}{R^2}\int_a^R r\,\mathrm{d}r\left[\theta'(r)^2 + \frac{\sin^2\theta(r)}{r^2}\right]. \tag{7}$$

Let us calculate the magnetostatic energy. For the vortex distribution (6) the volume magnetostatic charges are absent ($\nabla\cdot\boldsymbol{m}=0$), and the surface contribution (1) can be presented in the form [12,13]

$$W_{\text{MS}}^{\text{vortex}} = \frac{2\pi}{\varepsilon}\int_0^\infty \mathrm{d}x(1-\mathrm{e}^{-2\varepsilon x}) \times\left[\int_\alpha^1 \rho\,\mathrm{d}\rho\cos\theta(\rho)J_0(\rho x)\right]^2. \tag{8}$$

The function $\theta(\rho)$, which minimises the total energy functional, is the solution of the integro-differential equation [13], which can be analysed only approximately. There are known several models for describing the vortex structure in the disk-shaped particles. We should mention the core model by Usov and Peschany [14] and its modifications [6,13,15,16], where the magnetostatic interaction was taken into account only through the core radius; also these models have a singularity at the core radius. More realistic model was proposed by Höllinger et al. [5], where the vortex has a bell-shaped structure, generalising the ansatz by Feldtkeller and Thomas [17] (see also [2, p. 265]). This model is in a good agreement with simulations data for a disk. Nevertheless, we will use another model by the following reasons: (i) the model should be able to describe magnetisation distributions both in disks and rings, and (ii) it should be very simple to be treated analytically. All mentioned above models cannot be simply generalised for the ring case, and cannot be analysed analytically.

In pursuance of above-mentioned reasons we propose the following *two-parameters Ansatz*:

$$\cos\theta(r) = \mu\exp\left[-\left(\frac{r}{\lambda l_{\text{ex}}}\right)^2\right]. \tag{9}$$

Here, parameter μ describes the vortex amplitude in the centre of the ring. The typical vortex width is determined by the parameter λ. An advantage of this ansatz is a possibility to describe different kinds of vortices: the OPV for $\mu=1$, the IPV for $\mu=0$, and the IMV for $\mu\in(0,1)$. For the case of the disk ($\mu=1$) our ansatz (9) fits well the structure of the pure OPV in easy-plane magnets [18].

For the analytical treatment of the model, we make also one serious simplification: we use the local shape-anisotropy model [19–21] instead of the nonlocal magnetostatic energy (8), what is acceptably for thin particles ($\varepsilon\ll1$):

$$W_{\text{anis}} = \frac{4\pi}{R^2}\int_a^R r\,\mathrm{d}r\cos^2\theta(r). \tag{10}$$

Finally, the total energy density for the vortex state ring reads

$$W_{\text{IMV}} = \frac{4\pi l_{\text{ex}}^2}{R^2}\int_{a/\lambda l_{\text{ex}}}^{R/\lambda l_{\text{ex}}} x\,\mathrm{d}x \times\left[\frac{1}{x^2} + \mu^2\mathrm{e}^{-2x^2}\left(\frac{4x^2}{1-\mu^2\mathrm{e}^{-2x^2}} - \frac{1}{x^2} + \lambda^2\right)\right]. \tag{11}$$

This integral can be derived analytically, the explicit form is calculated in Appendix A. We have derived the energy

(11) using the local shape-anisotropical model (10) instead of the nonlocal magnetostatic one (8). Strictly speaking, the simplified model is valid only for infinitesimally thin rings, see Appendix B for details. However, further analysis demonstrates that it provides a reasonably accurate picture of phenomenon even for a large aspect ratio.

3.1. Pure OPV

We start our analysis with the case of a disk-shaped nanoparticle, where the pure OPV is realised. This well-known case is a good test for our simple theory. The magnetisation in the vortex centre is perpendicular to the disk plane, therefore, the vortex amplitude at origin is equal to unit, $\mu = 1$.

The energy of the vortex state nanodisk can be easily derived as a limit case of Eq. (11), see Appendix A for details:

$$W_{\mathrm{OPV}} = \frac{2\pi l_{\mathrm{ex}}^2}{R^2}\left[\gamma - \frac{1}{2}\xi_R^2 - \mathrm{Ei}(-\xi_R) + \ln\xi_R + \xi_R \ln(\mathrm{e}^{\xi_R} - 1) - \int_1^{\mathrm{e}^{\xi_R}} \frac{\ln(t-1)}{t}\,\mathrm{d}t\right] + 2\pi\frac{1-\mathrm{e}^{-\xi_R}}{\xi_R}. \tag{12}$$

Here $\xi_R = 2R^2/\lambda^2 l_{\mathrm{ex}}^2$, $\gamma \simeq 0.577$ is Euler's constant; $\mathrm{Ei}(\xi)$ is the exponential integral function [9]. The value of the variational parameter λ can be found by the minimisation of the energy (12) with respect to λ. Finally, the λ-parameter can be calculated as a solution of transcendental equation

$$\lambda^2(R) = 2\frac{1 + \mathrm{e}^{-2\xi_R} + \mathrm{e}^{-\xi_R}(\xi_R^2 - 2)}{1 + \mathrm{e}^{-2\xi_R}(1+\xi_R) - \mathrm{e}^{-\xi_R}(\xi_R + 2)}, \tag{13}$$

which can be solved numerically. For the case of large enough disk radii ($R > 4l_{\mathrm{ex}}$), the numerical solution $\lambda(R)$ practically coincides (with the accuracy within 2×10^{-5}) with the limit value $\lambda(\infty) = \sqrt{2}$.

To verify our analytical model calculations we have performed the numerical computer simulations using a three-dimensional OOMMF micromagnetic simulator code [22]. In all simulations we have used the following material parameters for the Py: $A = 1.3\times10^{-6}$ erg/cm (using SI units $A^{\mathrm{SI}} = 1.3\times10^{-11}$ J/m), $M_{\mathrm{s}} = 8.6\times10^{2}$ G ($M_{\mathrm{s}}^{\mathrm{SI}} = 8.6\times10^{5}$ A/m), and the anisotropy have been neglected. This corresponds to the exchange length $l_{\mathrm{ex}} = \sqrt{A/4\pi M_{\mathrm{s}}^2} \approx 5.3$ nm ($l_{\mathrm{ex}}^{\mathrm{SI}} = \sqrt{A/\mu_0 M_{\mathrm{s}}^2}$). A comparison of the vortex profiles, obtained by simulations and by analytical approach is presented in Fig. 2. Our ansatz (9) fits the simulation data with the accuracy within 0.09.

3.2. Intermediate vortex solution

Let us consider the ring-shaped nanoparticle. The presence of the hole in the centre of the disk changes the topological properties of the vortex solution. Hence it is not necessary for the vortex amplitude to be equal to unit in the ring centre. Moreover, if the inner hole is big enough, there can exist pure IPV, where the magnetisation does not have out-of-plane component at all. In the intermediate case of small enough inner hole the vortex amplitude μ should vary in the range [0, 1]. We have verified this idea by the micromagnetic simulations, as described above. One can see from Fig. 3 that the OPV structure has a well-defined bell shape, but the amplitude of the vortex decays fast when the inner hole becomes bigger. When the inner hole is greater than some critical value a_{c}, which is about 2 nm for the Py ring, only pure IPV solutions can be realised.

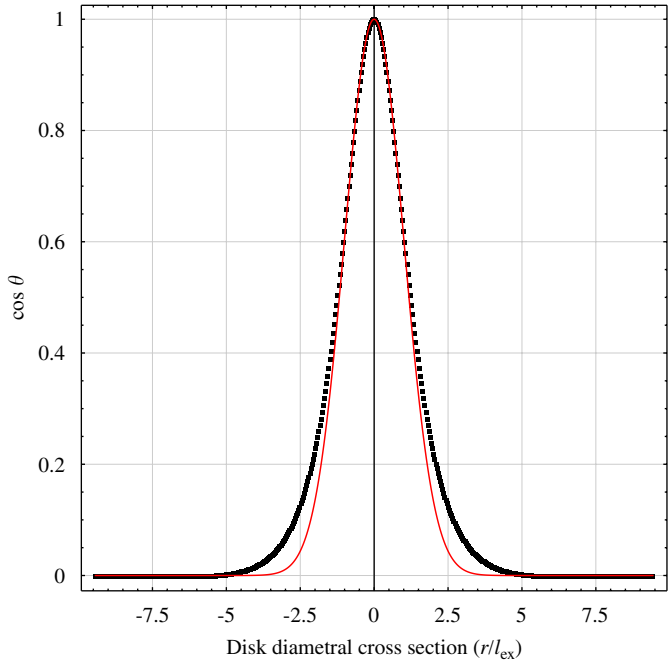

Fig. 2. The comparison of two OPV profiles: the ansatz (9) with $\mu = 1$ and $\lambda = \sqrt{2}$ (solid red line) and micromagnetic simulations (black bars) for the Py disk ($R = 50$ nm, $h = 5$ nm).

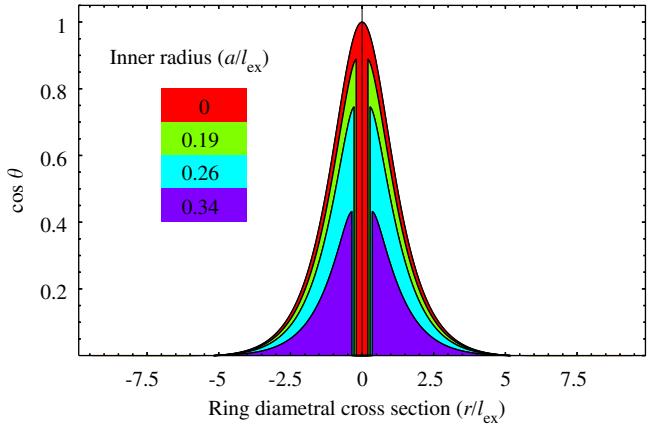

Fig. 3. Micromagnetic simulation data of the IMV profiles for different radii of inner hole. Other parameters are the same as in Fig. 2.

We have chosen the ansatz (9) because the bell shapes of the vortex structures are well pronounced for different vortex amplitudes. Using this ansatz we have derived the general expression for the vortex energy (11). To calculate variational parameters of our model μ and λ, we have minimised the energy (9) with respect to these parameters: $\partial W/\partial\mu = 0$ and $\partial W/\partial\lambda = 0$. This set of equations can be solved only numerically. Analysis shows that the solution practically (with the accuracy within 1×10^{-4}) does not depend on R when $R > 3l_{ex}$, hence one can use the limit case $R \to \infty$ in calculations. The results are presented in Fig. 4. Both analytical and simulation results have the same main behaviour: the vortex amplitude slightly decays when the inner hole increases for small enough holes, but it sharply breaks at some critical inner radius a_c. However, the value of the critical inner radius is about 2 nm from simulations while $a_c = 1.6$ nm from the theory (see below). This discrepancy in critical values is caused by the local model of the magnetostatic interaction. In Appendix B we will take into account the nonlocal magnetostatic interaction, which gives the critical inner radius 1.94 nm, what is in a good agreement with simulations results. Note that in real spin systems the vortex amplitude is always smaller than unit due to discreteness effects [23]; it means that the inner hole can never be smaller than the lattice constant a_0. In this context it is instructive to interpret our results also for the discrete systems, where the inner hole plays the role of the lattice constant. It is well known [23] that for anisotropic magnets there exists the transition from the OPV to IPV when the anisotropy changes. The transition occurs when the magnetic length ℓ (analogue of l_{ex}) goes down to the value about a_0 in analogy with our transition, see Fig. 4.

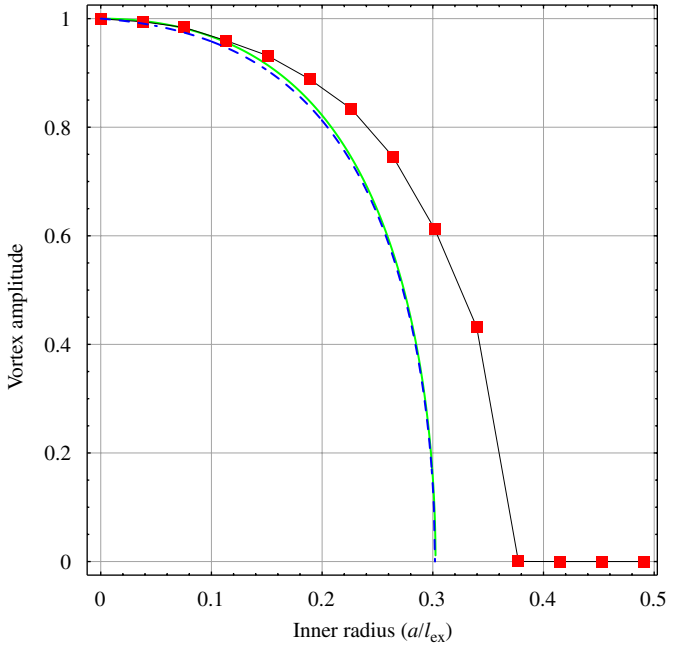

Fig. 4. Vortex amplitude (at the inner edge) vs. inner radius of the ring. Bars denote simulations results and solid green line corresponds to theoretical calculation, which were performed numerically. Dashed blue line corresponds to the fit (16). Other parameters are the same as in Fig. 2.

To calculate the critical value a_c, when the transition to IPV occurs, one can expand the IMV energy density (11) in series on μ at $\mu = 0$:

$$W_{IMV} \approx \frac{\mu^2}{2} C_1(\lambda) + \frac{\mu^4}{4} C_2(\lambda),$$

$$C_1(\lambda) = \frac{8\pi l_{ex}^2}{R^2} \int_{a/\lambda l_{ex}}^{\infty} dx\, x e^{-2x^2} \left(4x^2 - \frac{1}{x^2} + \lambda^2\right),$$

$$C_2(\lambda) = \frac{64\pi l_{ex}^2}{R^2} \int_{a/\lambda l_{ex}}^{\infty} dx\, x^3 e^{-4x^2}. \tag{14}$$

One can see that C_2 is always positive, hence the vortex solution with $\mu \neq 0$ can exist only when $C_1 < 0$. This is the case of the double-well potential with minima at $\mu^2 = |C_1|/C_2$. The pure IPV solution with $\mu = 0$ corresponds to the case of $C_1 > 0$. Thus, the critical point can be found from the condition $C_1 = 0$. The numerical solution of the equation

$$\int_{a/\lambda l_{ex}}^{\infty} dx\, x e^{-2x^2} \left(4x^2 - \frac{1}{x^2} + \lambda^2\right) = 0 \tag{15}$$

is shown in Fig. 5. It is not necessary to check the second minimum condition with respect to λ. Obviously, the critical parameters correspond to the maximum of the curve $a(\lambda)$. Finally, the critical inner radius $a_c \approx 0.3 l_{ex}$, see Appendix A.

At vicinity of the critical point, the vortex amplitude has asymptotic $\mu \propto \sqrt{a_c - a}$. One can extend this result and use the function

$$\mu^{approx} = \sqrt{\frac{1 - a/a_c}{(1 - a/l_{ex})^3}}, \tag{16}$$

which fits the numerical results of Fig. 4 with high accuracy (about 9×10^{-3}) in the whole range of the parameters.

When the inner ring radius a exceeds the critical value a_c, the pure IPV solution with $\mu = 0$ takes place. In this case all magnetostatic charges are absent, and the vortex energy

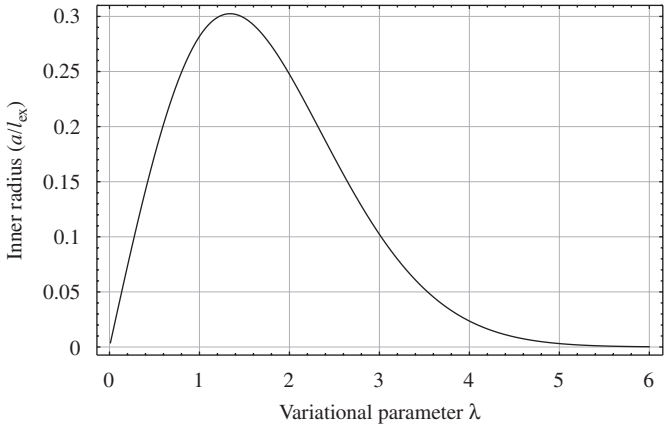

Fig. 5. The numerical solution of Eq. (15).

density has only exchange contribution, which simply reads

$$W_{\mathrm{IPV}} = \frac{4\pi l_{\mathrm{ex}}^2}{R^2} \ln\frac{R}{a}. \tag{17}$$

4. Phase diagrams

Summarising results on the equilibrium magnetisation distribution, we have calculated energetically preferable states for different ring geometries. Since we have three parameters, which define the ring, R, a, and h, our phase diagram is a three-dimensional plot. Theoretically calculated phase diagram is presented in Fig. 6. Different phases are separated by boundary surfaces. The general properties of the phase diagram are as follows. The ground state of the very thin ring is the homogeneous easy-plane state. As the thickness increases we can switch to the homogeneous easy-axis state, when the outer ring radius is small enough, or to the vortex state, when the ring is large. The boundary surface between two homogeneous states can be simply expressed analytically, $h = 2R\varepsilon_{\mathrm{c}}(\alpha)$, where the $\varepsilon_{\mathrm{c}}(\alpha)$-dependence is described by Eq. (5), see also Fig. 1. Now, if we increase the inner radius of the ring, the vortex state becomes energetically preferable. One can follow step-by-step transitions between different vortex phases: from the pure OPV state for the case of the disk ($a = 0$) to the IMV state for the ring with small radii ratio ($a < a_{\mathrm{c}}$) and, finally, to the pure IPV state when $a > a_{\mathrm{c}}$.

To verify our theoretically calculated phase diagram, we use 3D micromagnetic simulations, as described above. Simulations data are reproduced in Fig. 7 together with theoretical results. Fig. 7a presents the phase diagram for the case of the nanodisk. Numerical results for this case are in a good agreement with previous theoretical [6,15] and experimental [7] results. One can compare the theoretical results obtained within the local (solid line) and nonlocal (dashed line) models of the magnetostatic interaction. In the case of thin disks the boundaries are coincident and agree with simulations results. However, in the case of thick disks for the boundary between OPV phase and homogeneous EA solid line (the local model) lies higher then simulations data. This is because the variational approach in the local shape-anisotropy model always gives the upper limit of the energy.

The presence of the hole inside the disk drastically changes the vortex state. The vortex amplitude depends on the inner radius of the ring. If the radii ratio is small enough, the phase diagram contains four phases, see Fig. 7b. The boundary between phases IMV and IPV was calculated using nonlocal model of magnetostatic interaction (see Appendix B). We have not managed to calculate the boundaries between homogenous and vortex states within nonlocal model, because in the case of ring there are two variational parameters (μ and λ), in contrast to the case of disk, where only one variational parameter (λ) is present. If the inner radius exceeds the critical value a_{c}, only one vortex phase with IPVs can exist, see Figs. 7c and d.

The *triple* point in the phase diagrams is the object of a special interest. In particular, it provides an information about the lowest possible radius of the vortex state nanoparticle. The triple point was analysed for the disk particles using the scaling technique [16,24]. Here, we present results for the case of the ring. Since at this point the vortex energy W_{IMV} is equal to the homogeneous state energies, moreover $W_{\mathrm{MS}}^x = W_{\mathrm{MS}}^z$, one can calculate the triple point parameters by solving an equation $W_{\mathrm{IMV}} = 2\pi/3(1-\alpha^2)$. In general case it can be done numerically only, see Fig. 8. An analytical analysis can be performed asymptotically for small α, where we can limit ourselves to the linear dependence $2R^{(\mathrm{tr})} = h^{(\mathrm{tr})}/\varepsilon_0$, where $\varepsilon_0 \approx 0.906$ is the critical aspect ratio for a disk [10]. In the limit case of $\alpha = 0$ the triple point is characterised by the following parameters: $R^{(\mathrm{tr})} \approx 3.73 l_{\mathrm{ex}}$ and $h^{(\mathrm{tr})} \approx 6.76 l_{\mathrm{ex}}$.

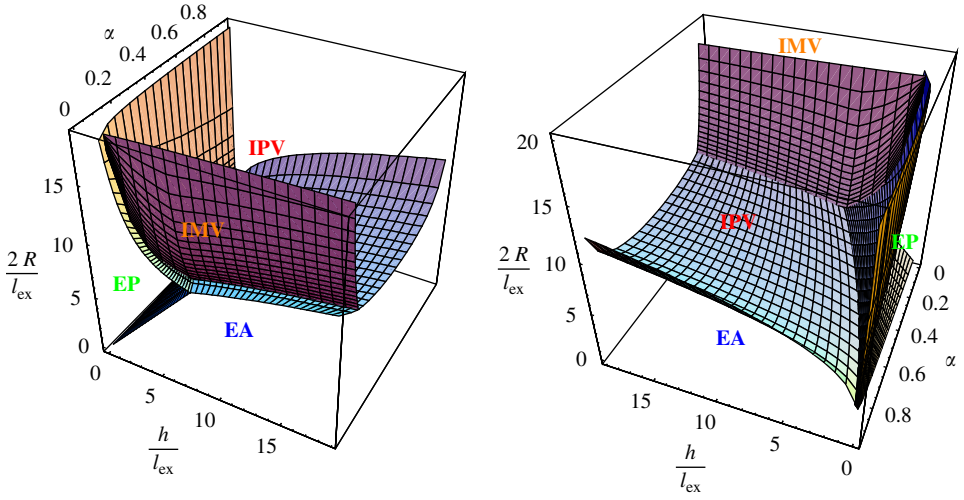

Fig. 6. Three-dimensional phase diagram of magnetisation ground states from analytical analysis.

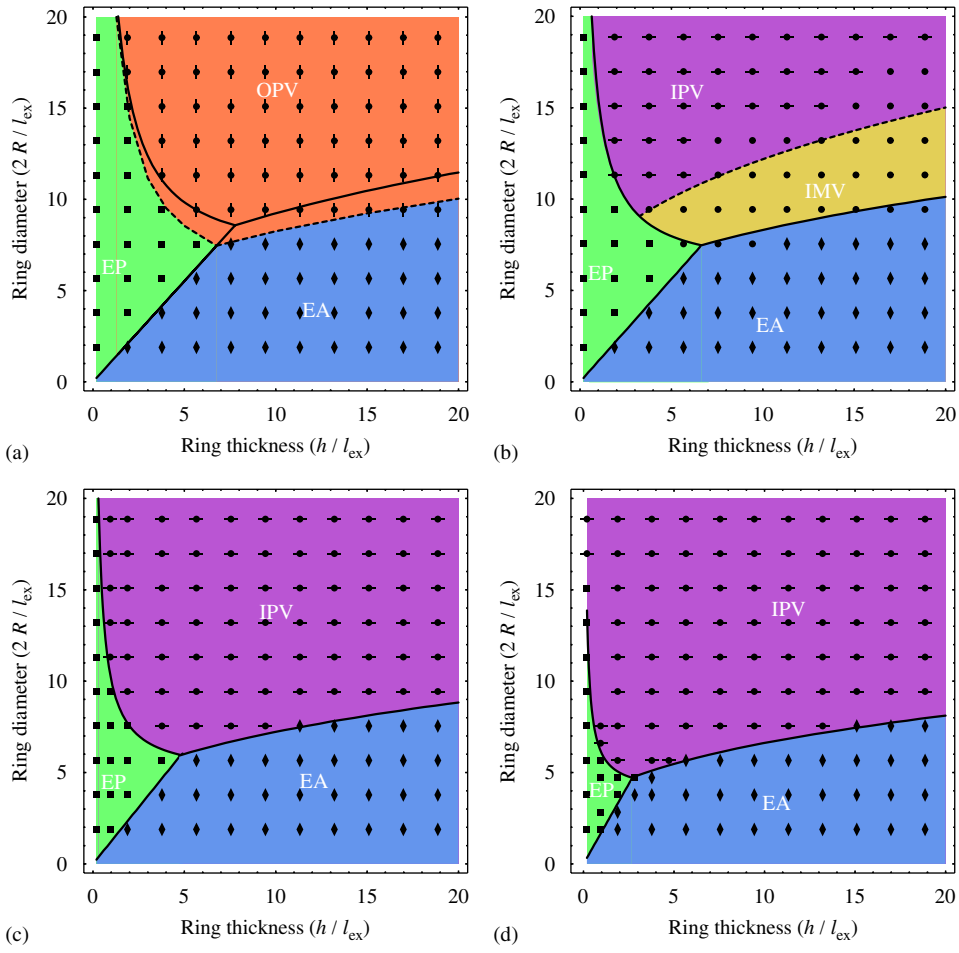

Fig. 7. The phase diagrams of magnetic ground states for different radii ratio: (a) $\alpha = 0$; (b) $\alpha = 0.1$; (c) $\alpha = 0.25$ and (d) $\alpha = 0.5$. The areas of different colours correspond to different kinds of magnetisation distribution. Symbols represent the simulation data: squares—EP, diamonds—EA, disks—IMV, disks with vertical lines—OPV, disks with horizontal lines—IPV. The dashed lines in (a) and (b) are the theoretical borders calculated within the nonlocal model of magnetostatic interaction. Solid lines correspond to the theoretical borders, calculated within the local model.

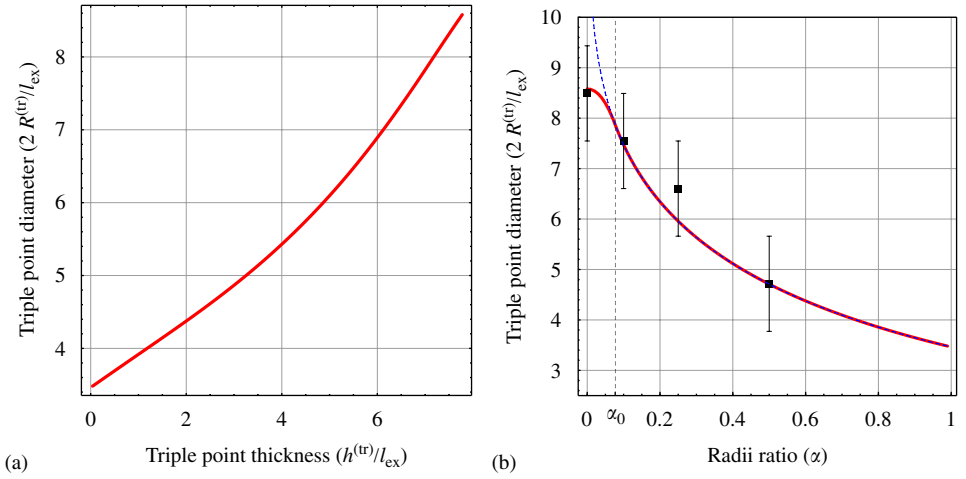

Fig. 8. The triple point analysis: the outer ring diameter as a function of (a) the ring thickness and (b) the radii ratio. Red lines correspond to the exact numerically calculated data (the local model of the magnetostatics), dashed blue line is the analytical solution (18), which is acceptable for $\alpha > \alpha_0$. Points with error bars were obtained from simulations data (Fig. 7).

(The values were obtained for the nonlocal model of the magnetostatics.) By increasing the inner radius, the triple point radius $R^{(tr)}$ decreases, so the IMV can exist in smaller particles than the pure OPV. At some critical inner radius a_c the transition to the IPV state occurs. The energy of the pure IPV has a simple form (17), so the triple point analysis

can be easily done for this case:

$$R^{(\mathrm{tr})}(\alpha) = l_{\mathrm{ex}}\sqrt{\frac{6}{1-\alpha^2}\ln\frac{1}{\alpha}}, \quad h^{(\mathrm{tr})}(\alpha) = 2R^{(\mathrm{tr})}(\alpha)\varepsilon_{\mathrm{c}}(\alpha), \quad \alpha > \alpha_0, \tag{18}$$

where $\varepsilon_{\mathrm{c}}(\alpha)$-dependence is described by Eq. (5). Such simple analytical description of the triple point is valid only, when $a > a_{\mathrm{c}}$ and the IPV is stable. Simple calculations show that it can be realised for $\alpha > \alpha_0 \approx 0.077$. The triple point radius $R^{(\mathrm{tr})}$ and thickness $h^{(\mathrm{tr})}$ diminish when α increases, and they have the asymptotic behaviour:

$$R^{(\mathrm{tr})}(\alpha) \underset{\alpha\to 1}{\sim} l_{\mathrm{ex}}\sqrt{3}[1 + (1-\alpha)/2],$$
$$h^{(\mathrm{tr})}(\alpha) \underset{\alpha\to 1}{\sim} 2l_{\mathrm{ex}}\sqrt{3}(1-\alpha). \tag{19}$$

The limit value $R^{(\mathrm{tr})}(1) = l_{\mathrm{ex}}\sqrt{3}$ provides the lowest bound for the vortex state magnetic ring. For the Py nanoring this limit is about 9.18 nm.

5. Conclusions

We have presented a detailed study of the ground state of magnetic nanorings, including homogeneous (easy-axis and easy-plane) states and inhomogeneous vortex states. In addition to conventional OPV and IPV types we have found a new type of vortices in a nanoring. Such intermediate vortices are characterised by the smaller amplitude in the vortex centre, they are the key point to understand the transition from OPV to IPV state. We have proposed also a simple analytical description of the IMV state. Using this approach we have studied analytically phase transitions between different ground states. All results are confirmed by our direct 3D micromagnetic simulations.

Using the critical analysis of the phase diagram triple point, we conclude that the lower bound of the vortex-state nanoparticle decreases for a ring geometry in comparison with a disk. The minimal nanoring radius varies from about $3.7l_{\mathrm{ex}}$ for the case of the disk to $\sqrt{3}l_{\mathrm{ex}}$ for the case of narrow ring.

It is necessary to mention here that all our conclusions are based on the ground energy calculations. However, the boundaries can be influenced by the stability ranges of different phases. Stability lines due to the vortex shifts were studied in Refs. [12,13]. The magnetic bistability of single domain and vortex states was studied recently both theoretically and experimentally in Ref. [25]. This leads to the finite width of the boundaries in phase diagrams.

Our model of the IMV can be applied for the description of dynamical effects of the switching of the vortex polarisation [26–28]. We expect that the dynamical switching effects should be more pronounced in the ring geometry, because the vortex amplitude μ can smoothly vary and even change its sign. This is the subject of future research.

Acknowledegments

Authors acknowledge the support from Deutsches Zentrum für Luft-und Raumfart e.V., Internationales Büro des BMBF in the frame of a bilateral scientific cooperation between Ukraine and Germany, project no. UKR 05/055. All simulations results presented in the work were obtained using the computing cluster of Kiev University [29]. V.Kr. thanks O. Sudakov for productive consultations about the computing cluster using. D. Sh. thanks the University of Bayreuth, where part of this work was performed, for kind hospitality and acknowledges support from the Alexander von Humboldt Foundation.

Appendix A. The vortex state energy calculations

Let us start with the vortex energy in the form (11). Using the direct integration one can write down the energy in the form

$$W_{\mathrm{IMV}} = \frac{2\pi l_{\mathrm{ex}}^2}{R^2}[\mathscr{I}(\xi_a) - \mathscr{I}(\xi_R)]. \tag{A.1}$$

Here, $\xi_a = 2a^2/l_{\mathrm{ex}}^2\lambda^2$ and $\xi_R = 2R^2/l_{\mathrm{ex}}^2\lambda^2$; the integral $\mathscr{I}(\xi)$ can be expressed as follows:

$$\mathscr{I}(\xi) = \frac{\xi^2}{2} + \frac{\lambda^2\mu^2}{2}\mathrm{e}^{-\xi} + \mu^2\mathrm{Ei}(-\xi) + \int_1^{\mathrm{e}^{\xi}/\mu^2}\frac{\ln(t-1)}{t}\,\mathrm{d}t - \ln\xi - \xi\ln\left(\frac{\mathrm{e}^{\xi}}{\mu^2} - 1\right), \tag{A.2}$$

where $\mathrm{Ei}(x)$ is the exponential integral function.

Using the asymptotical behaviour

$$\mathscr{I}(\xi) \underset{\xi\to 0}{\sim} \frac{\lambda^2\mu^2}{2} + \mu^2\gamma - \ln\xi(1-\mu^2) + \int_1^{1/\mu^2}\frac{\ln(t-1)}{t}\,\mathrm{d}t, \tag{A.3}$$

one can easily calculate that $\mathscr{I}(0) = \lambda^2/2 + \gamma$ when $\mu = 1$. According to (A.1) the vortex energy of a disk with radius R can be written down as

$$W_{\mathrm{OPV}} = \frac{2\pi l_{\mathrm{ex}}^2}{R^2}[\mathscr{I}(0) - \mathscr{I}(\xi_R)]_{\mu=1}, \tag{A.4}$$

which results in (12).

Let us go back to the case of the ring and calculate the critical inner radius, when the transition from the IMV solution to the pure in-plane one takes place. One can rewrite Eq. (15) as follows:

$$F(a,\lambda) = \int_{a/\lambda l_{\mathrm{ex}}}^{\infty}\mathrm{d}x\; x\,\mathrm{e}^{-2x^2}\left(4x^2 - \frac{1}{x^2} + \lambda^2\right) = 0, \tag{15′}$$

which is an implicit form of the dependence $a(\lambda)$. The critical value a_{c} can be calculated from the condition $\partial F/\partial\lambda = 0$; hence $a_{\mathrm{c}} = l_{\mathrm{ex}}\sqrt{x_0 - x_0^2}$, where x_0 is a positive root of the equation $2\mathrm{e}^{-x} + \mathrm{Ei}(-x) = 0$. This results in $x_0 \approx 0.1$ and $a_{\mathrm{c}} \approx 0.3l_{\mathrm{ex}}$.

Appendix B. Magnetostatic energy calculations

Let us write down an expression for the vortex energy with account of the nonlocal magnetostatic contribution (8):

$$W_{\mathrm{IMV}} = \frac{4\pi l_{\mathrm{ex}}^2}{R^2}\int_{a/\lambda l_{\mathrm{ex}}}^{R/\lambda l_{\mathrm{ex}}} x\,\mathrm{d}x\left[\frac{1}{x^2}+\mu^2\mathrm{e}^{-2x^2}\left(\frac{4x^2}{1-\mu^2\mathrm{e}^{-2x^2}}-\frac{1}{x^2}\right)+\lambda^2\mu^2\mathscr{K}\left(x,\frac{a}{\lambda l_{\mathrm{ex}}},\frac{R}{\lambda l_{\mathrm{ex}}},\frac{h}{\lambda l_{\mathrm{ex}}}\right)\right]. \tag{B.1}$$

Here, the kernel of integral

$$\mathscr{K}(x,\xi,\eta,\zeta) = \frac{\mathrm{e}^{-x^2}}{\zeta}\int_{\xi}^{\eta} x'\mathrm{e}^{-x'^2} \times \int_0^{\infty}(1-\mathrm{e}^{-\zeta t})J_0(xt)J_0(x't)\,\mathrm{d}t\,\mathrm{d}x'. \tag{B.2}$$

Note that in the limit case of thin films $\mathscr{K}(x,\xi,\eta,\zeta\to 0)\to\exp(-2x^2)$, see Ref. [13], which corresponds to the local model (11).

An account of nonlocal magnetostatic interaction changes the value of the critical inner radius, when the magnetic phase transition into the pure IPV phase occurs. This critical radius can be calculated numerically as a solution of the following equation:

$$\int_{a/\lambda l_{\mathrm{ex}}}^{\infty}\mathrm{d}x\;x\left[\mathrm{e}^{-2x^2}\left(4x^2-\frac{1}{x^2}\right)+\lambda^2\mathscr{K}\left(x,\frac{a}{\lambda l_{\mathrm{ex}}},\infty,\frac{h}{\lambda l_{\mathrm{ex}}}\right)\right]=0. \tag{B.3}$$

To simplify the numerical calculations one can reduce the kernel to

$$\mathscr{K}(x,\xi,\infty,\zeta) = \frac{2\mathrm{e}^{-x^2}}{\pi\zeta}\left\{\int_{\xi}^{x}\frac{t\mathrm{e}^{-t^2}K(t/x)}{x}\,\mathrm{d}t+\int_{x}^{\infty}\mathrm{e}^{-t^2}K(x/t)\,\mathrm{d}t - \int_{\xi}^{\infty}\frac{t\mathrm{e}^{-t^2}K(2\sqrt{tx}/\sqrt{\zeta^2+(x+t)^2})}{\sqrt{\zeta^2+(x+t)^2}}\,\mathrm{d}t\right\}, \tag{B.4}$$

where K(x) is the elliptical integral of the first kind.

The solution of the Eq. (B.3) with kernel (B.4) is shown in Fig. B1. The maximum of dependence $a(\lambda)$ that corresponds to the critical value of inner radius is $a_{\mathrm{c}}\approx 0.37 l_{\mathrm{ex}}$. For the Py nanoring $a_{\mathrm{c}}\approx 1.94$ nm, which agrees with the simulations data, see Fig. 4.

An account of nonlocal interaction gives a possibility to calculate the critical inner radius on thickness of the ring, see Fig. B2. This dependence can be fitted by the function

$$a_{\mathrm{c}}^{\mathrm{fit}}(h)\approx a_{\mathrm{c}}\sqrt[3]{1+ch/l_{\mathrm{ex}}},\quad c\approx 0.68, \tag{B.5}$$

where $a_{\mathrm{c}}\approx 0.37 l_{\mathrm{ex}}$ is the limit value for infinitesimally thin rings, which was calculated in Section 3. We also have numerically calculated the dependence of vortex width (λ) on disk thickness (for nonlocal magnetostatic model), see Fig. B3.

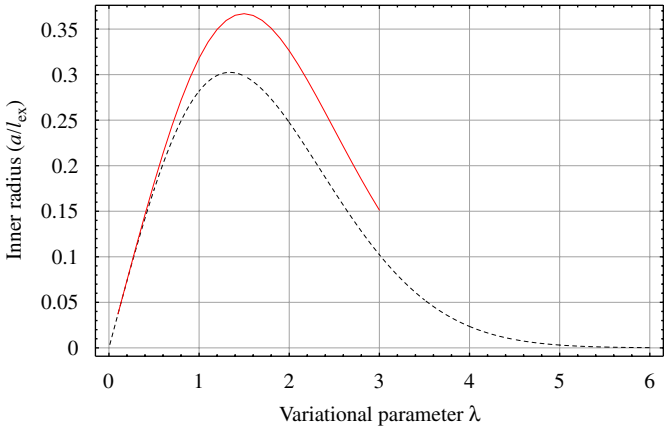

Fig. B1. The numerical solution of the Eq. (B.3) is denoted by solid red line. During the calculation it was assumed that parameter $h/l_{\mathrm{ex}} = 5\,\mathrm{nm}/5.3\,\mathrm{nm}$, that corresponds to the parameters of the simulations (see Fig. 4). Dashed black line corresponds to the solution of the model of local magnetostatics (15), Fig. 5.

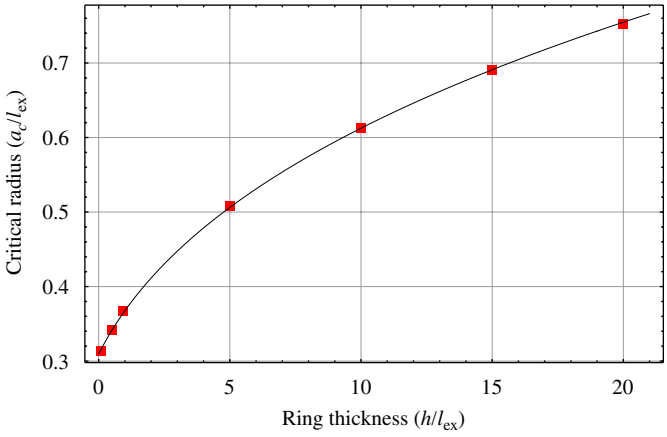

Fig. B2. The dependence of the critical inner radius on thickness of the ring. Red bars denote the exact values, which were obtained numerically. Solid black line corresponds to the fit (see text).

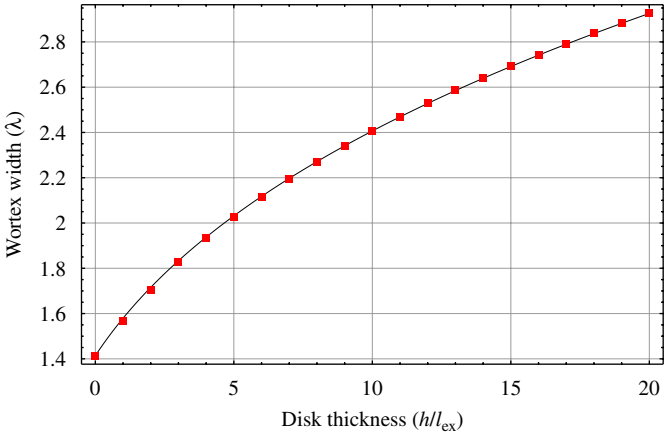

Fig. B3. The dependence of the vortex width in case of disk on disk thickness.

This dependence also can be well fitted by the third-root function:

$$\lambda^{\mathrm{fit}}(h) \approx \sqrt{2}\sqrt[3]{1 + dh/l_{\mathrm{ex}}}, \quad d \approx 0.39. \tag{B.6}$$

References

[1] R. Skomski, J. Phys. C 15 (2003) R841 URL: ⟨http://www.iop.org/EJ/abstract/0953-8984/15/20/202/⟩.

[2] A. Hubert, R. Schäfer, Magnetic Domains, Springer, Berlin, 1998.

[3] R.P. Cowburn, J. Magn. Magn. Mater. 242–245 (2002) 505 URL: ⟨http://www.sciencedirect.com/science/article/B6TJJ-44NM486-19%/2/d76afadecc91907bb34369038cc8368e⟩.

[4] R.P. Cowburn, D.K. Koltsov, A.O. Adeyeye, M.E.W. D.M. Tricker, Phys. Rev. Lett. 83 (1999) 1042.

[5] R. Höllinger, A. Killinger, U. Krey, J. Magn. Magn. Mater. 261 (2003) 178 URL: ⟨http://www.sciencedirect.com/science/article/B6TJJ-47F1D5K-1/%2/02a9f675dac9cbb50d643664d50b98be⟩.

[6] W. Scholz, K.Y. Guslienko, V. Novosad, D. Suess, T. Schrefl, R.W. Chantrell, J. Fidler, J. Magn. Magn. Mater. 266 (2003) 155 URL: ⟨ http://www.sciencedirect.com/science/article/B6TJJ-48XJG14-2/%2/99674233c0c57efed3e8c330363537c0⟩.

[7] C.A. Ross, M. Hwang, M. Shima, J.Y. Cheng, M. Farhoud, T.A. Savas, H.I. Smith, W. Schwarzacher, F.M. Ross, M. Redjdal, et al., Phys. Rev. B 65 (2002) 144417 URL: ⟨http://link.aps.org/abstract/PRB/v65/e144417⟩.

[8] M. Kläui, C.A.F. Vaz, L. Lopez-Diaz, J.A.C. Bland, J. Phys.: Condens. Matter 15 (2003) R985.

[9] M. Abramowitz, I.A. Stegun, Handbook of Mathematical Functions with Formulas, Graphs, and Mathematical Tables, Dover, New York, 1964, ninth Dover printing, tenth gpo printing ed., ISBN 0-486-61272-4.

[10] A. Aharoni, J. Appl. Phys. 68 (1990) 2892 URL: ⟨http://link.aip.org/link/?JAP/68/2892/1⟩.

[11] A.I. Akhiezer, V.G. Bar'yakhtar, S.V. Peletminskiĭ, Spin Waves, North-Holland, Amsterdam, 1968.

[12] N.A. Usov, S.E. Peschany, Fiz. Met. Metalloved. 78 (1994) 13 (in Russian).

[13] K.Y. Guslienko, V. Novosad, J. Appl. Phys. 96 (2004) 4451 URL: ⟨http://link.aip.org/link/?JAP/96/4451/1⟩.

[14] N.A. Usov, S.E. Peschany, J. Magn. Magn. Mater. 118 (1993) L290 URL: ⟨http://www.sciencedirect.com/science/article/B6TJJ-46FHH1R-C8%/2/24f0bbd22588428bbea2c69d514bc837⟩.

[15] K.L. Metlov, K.Y. Guslienko, J. Magn. Magn. Mater. 242–245 (2002) 1015 URL: ⟨http://www.sciencedirect.com/science/article/B6TJJ-44PKP2R-F/%2/3cb3318ef44a490869eeae7cf4d79650⟩.

[16] P. Landeros, J. Escrig, D. Altbir, D. Laroze, J. d'Albuquerque e Castro, P. Vargas, Phys. Rev. B 71 (2005) 094435 URL: ⟨http://link.aps.org/abstract/PRB/v71/e094435⟩.

[17] E. Feldtkeller, H. Thomas, Phys. Kond. Mater. 4 (1965) 8.

[18] F.G. Mertens, A.R. Bishop, in: P.L. Christiansen, M.P. Soerensen, A.C. Scott (Eds.), Nonlinear Science at the Dawn of the 21th Century, Springer, Berlin, 2000.

[19] G. Gioia, R.D. James, Proc. R. Soc. London Ser. A 453 (1997) 213 URL: ⟨http://www.journals.royalsoc.ac.uk/openurl.asp?genre=article&%id=doi:10.1098/rspa.1997.0013⟩.

[20] B.A. Ivanov, C.E. Zaspel, Appl. Phys. Lett. 81 (2002) 1261.

[21] D.D. Sheka, J.P. Zagorodny, J.G. Caputo, Y. Gaididei, F.G. Mertens, Phys. Rev. B 71 (2005) 134420 URL: ⟨http://link.aps.org/abstract/PRB/v71/e134420⟩.

[22] The Object Oriented MicroMagnetic Framework, URL: ⟨http://math.nist.gov/oommf/⟩.

[23] G.M. Wysin, Phys. Rev. B 49 (1994) 8780 URL: ⟨http://link.aps.org/abstract/PRB/v49/p8780⟩.

[24] J. d'Albuquerque e Castro, D. Altbir, J.C. Retamal, P. Vargas, Phys. Rev. Lett. 88 (2002) 237202 URL: ⟨http://link.aps.org/abstract/PRL/v88/e237202⟩.

[25] H.F. Ding, A.K. Schmid, D. Li, K.Y. Guslienko, S.D. Bader, Phys. Rev. Lett. 94 (2005) 157202 URL: ⟨http://link.aps.org/abstract/PRL/v94/e157202⟩.

[26] Y. Gaididei, T. Kamppeter, F.G. Mertens, A.R. Bishop, Phys. Rev. B 61 (2000) 9449.

[27] R. Pulwey, M. Rahm, J. Biberger, D. Weiss, IEEE Trans. Magn. 37 (2001) 2076.

[28] J.P. Zagorodny, Y. Gaididei, F.G. Mertens, A.R. Bishop, Eur. Phys. J. B 31 (2003) 471.

[29] Kyiv National Taras Shevchenko University high-performance computing cluster, URL: ⟨http://www.unicc.kiev.ua/eng/⟩.